INTERNATIONAL JOURNAL FOR NUMERICAL METHODS IN ENGINEERING, VOL. 36, 1681–1701 (1993)

FRICTIONAL CONTACT FINITE ELEMENTS BASED ON MIXED VARIATIONAL PRINCIPLES

S. CESCOTTO AND R. CHARLIER

M.S.M. Department, Université de Liege, Quai Banning, 6, B-4000 Liege, Belgium

SUMMARY

This paper presents an original approach to the numerical modelling of unilateral contact by the finite element method. The main point is the development of mixed contact finite elements in which the displacement field and the contact stress field (pressure and friction shear) are discretized independently. The theory, based on variational principles, is first presented in the framework of infinitesimal deformations and, subsequently, is extended to large inelastic strains.

1. INTRODUCTION

The numerical modelling of unilateral contact with friction leads to a very wide variety of solutions, especially in the context of large strains. The main differences appear at two levels: the choice of a constitutive equation for contact (Coulomb, Tresca, etc.) and the algorithm used to solve the inequalities of contact (direct solution of the inequalities, penalty method, Lagrangian multipliers, augmented Lagrangian method, etc.).

A special issue of the *Journal of Theoretical and Applied Mechanics*,[1] specially devoted to unilateral contact modelling, gives an account of the present state of knowledge in this field.

Usually, in a finite element context, the contact inequalities are written in terms of nodal co-ordinates. For example, it is expressed that the finite element nodes belonging to the boundary of the discretized solid may not penetrate into a rigid second body, named here the foundation.

This approach can be qualified as 'compatible or displacement-type approach' since the discretized displacements of the solid are the basic variables.

However, it does not prevent the overlapping of the discretized solid and the foundation (Figure 1), even when the nodal inequalities are solved exactly.

In this paper, an alternative solution is proposed, in which the contact stresses and the displacement field on the solid boundary are discretized independently. It is based on mixed variational principles and allows to control the average overlapping between the solid boundary and the foundation.

It is also shown that, in some particular cases, the mixed contact finite elements based on this formulation are equivalent to underintegrated compatible elements in which the contact inequalities are expressed at integration points on the solid boundary (Figure 2). Such elements were developed previously[1,2] on an intuitive basis and proved to be very effective. They are given here a theoretical basis.

The basic advantage of such mixed contact elements is that the contact condition is naturally smoother than with the compatible approach. In the latter method, a stiffness or an out-of-balance force is attributed to a node only when contact has taken place. On the contrary, in the

0029–5981/93/101681–21$15.50

Received 22 July 1991
Revised 1 July 1992

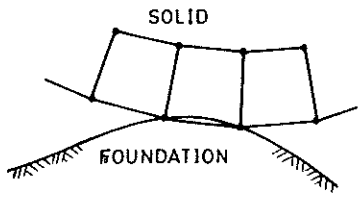

Figure 1

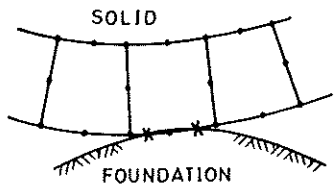

Figure 2

former method, it will be seen that a stiffness matrix and out-of-balance forces are computed for the mixed contact element, even when it is only partially in contact. In other words, a node which is not yet in contact but only close to contact is 'informed' by its neighbours that contact is going to occur soon.

The proposed discretization method does not have any influence of the interface rheology. The finite elements are based on the penalty method for solving the unilateral contact and slip conditions and on the Coulomb model for the friction strength. This approach has been extensively developed during the last ten years, especially in general incremental non-linear finite element codes (see for example References 1–5). Curnier[6] has made a nice synthesis of the contact and friction constitutive equations. More recently, some new developments[3,7,16] have been made on the penalty coefficients, which are based on experimental evidences. But the choice of the penalty coefficients remains a controversial question, which will not be discussed in this paper. Generally, it is required to keep the numerical values of the bodies penetration small relative to the finite element. Fluctuations of this penetration are related to the pressure variations along the contact surface. Separation between the bodies after contact is analysed on the basis of pressure evolution.

When slipping contact appears, the constitutive equation of the contact element is unsymmetric. Therefore, an unsymmetric solver is used.

The mixed approach is applied to the developments of a series of two-dimensional friction contact finite element. The extension to the three-dimensional state is straightforward.

Finally, two applications are presented. The first one is concerned with an axisymmetric forging problem and the second one with a three-dimensional shear-bond test.

2. MIXED VARIATIONAL PRINCIPLES

2.1. Hypotheses

For the sake of simplicity, we will start the development in a very restrictive framework: the deformable solid is linear elastic, its deformations are infinitesimal and the foundation is rigid.

Furthermore, it is assumed that the contact surface between the solid and the foundation is known and that no sliding is allowed (sticking contact).

Subsequently, these hypotheses will be removed in order to consider the case of an inelastic solid (elastoplastic, elastic viscoplastic) undergoing large strains, contact with sliding and friction, and unknown contact surface.

2.2. *Local and global co-ordinates*

We consider a solid of volume V and boundary A. Let A_U, A_T and A_C be the parts of A on which displacements, surface tractions and unilateral contact conditions are imposed, respectively. At each point S of A_C, local co-ordinates are defined (Figure 3), with $\mathbf{e}_1$ normal and $\mathbf{e}_2$, $\mathbf{e}_3$ tangent to A_C, which is assumed to be smooth. At point S, the displacement of the material particle of the solid, with respect to some reference configuration, is

$$\mathbf{u}_S = u_{Si}\mathbf{e}_i \tag{1}$$

and the stress tensor is denoted by $\boldsymbol{\sigma}_S$.

If p is the contact pressure and τ_1, τ_2 the contact shear stresses at point S, the surface equilibrium conditions give

$$\begin{aligned} \sigma_{S11} + p &= 0 \\ \sigma_{S21} + \tau_2 &= 0 \\ \sigma_{S31} + \tau_3 &= 0 \end{aligned} \tag{2}$$

where σ_{S11}, σ_{S21}, σ_{S31} are components of $\boldsymbol{\sigma}_S$ in the local frame $(\mathbf{e}_1, \mathbf{e}_2, \mathbf{e}_3)$.

Finally, if point S of the solid is in contact with point F of the rigid foundation, the displacement of the latter is:

$$\mathbf{u}_F = u_{Fi}\mathbf{e}_i \tag{3}$$

On the other hand, for internal points or for points belonging to A_U or A_T, we will use a global Cartesian reference system $\mathbf{E}_1, \mathbf{E}_2, \mathbf{E}_3$. For such points, the co-ordinates are X_1, X_2, X_3, and $\boldsymbol{\sigma}$, $\boldsymbol{\varepsilon}$, $\mathbf{u}$, $\mathbf{T}$, $\mathbf{F}$ are the stresses, strains, displacements, surface tractions and body forces, respectively, the components of which are expressed with respect to $\mathbf{E}_1$, $\mathbf{E}_2$, $\mathbf{E}_3$. For example,

$$\mathbf{u} = u_i\mathbf{E}_i \tag{4}$$

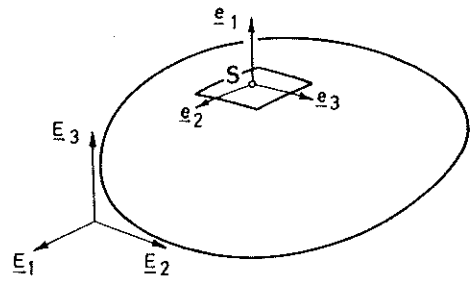

Figure 3

2.3. Matrix notation

For points belonging to A_C, the following notations will be used:

$$\boldsymbol{\sigma}_S = \begin{bmatrix} \sigma_{S11} \\ \sigma_{S21} \\ \sigma_{S31} \end{bmatrix}, \quad \boldsymbol{\sigma}_C \begin{bmatrix} p \\ \tau_2 \\ \tau_3 \end{bmatrix}$$

$$\mathbf{u}_S = \begin{bmatrix} u_{S1} \\ u_{S2} \\ u_{S3} \end{bmatrix}, \quad \mathbf{u}_F = \begin{bmatrix} u_{F1} \\ u_{F2} \\ u_{F3} \end{bmatrix}; \quad \boldsymbol{\varepsilon}_C = \mathbf{u}_S - \mathbf{u}_F$$

Hence, the surface equilibrium condition on A_C become

$$\boldsymbol{\sigma}_S + \boldsymbol{\sigma}_C = 0 \tag{5}$$

For points belonging to A_U, A_T or V, we will write

$$\boldsymbol{\sigma} = \begin{bmatrix} \sigma_{11} \\ \sigma_{22} \\ \sigma_{33} \\ \sigma_{23} \\ \sigma_{13} \\ \sigma_{12} \end{bmatrix}, \quad \boldsymbol{\varepsilon} = \begin{bmatrix} \varepsilon_{11} \\ \varepsilon_{22} \\ \varepsilon_{33} \\ 2\varepsilon_{23} \\ 2\varepsilon_{13} \\ 2\varepsilon_{12} \end{bmatrix}, \quad \partial\mathbf{u} = \begin{bmatrix} \partial u_1/\partial x_1 \\ \partial u_2/\partial x_2 \\ \partial u_3/\partial x_3 \\ \delta u_2/\partial x_3 + \partial u_3/\partial x_2 \\ \partial u_1/\partial x_3 + \partial u_3/\partial x_1 \\ \partial u_1/\partial x_2 + \partial u_2/\partial x_1 \end{bmatrix}$$

$$\mathbf{u} = \begin{bmatrix} u_1 \\ u_2 \\ u_3 \end{bmatrix}, \quad \mathbf{T} = \begin{bmatrix} T_1 \\ T_2 \\ T_3 \end{bmatrix}, \quad \mathbf{F} = \begin{bmatrix} F_1 \\ F_2 \\ F_3 \end{bmatrix}$$

$$\boldsymbol{\sigma}_n = \begin{bmatrix} n_1\sigma_{11} + n_2\sigma_{21} + n_3\sigma_{31} \\ n_1\sigma_{12} + n_2\sigma_{22} + n_3\sigma_{32} \\ n_1\sigma_{13} + n_2\sigma_{23} + n_3\sigma_{33} \end{bmatrix}, \quad \partial\boldsymbol{\sigma} = \begin{bmatrix} \partial\sigma_{11}/\partial x_1 + \partial\sigma_{21}/\partial x_2 + \partial\sigma_{31}/\partial x_3 \\ \partial\sigma_{12}/\partial x_1 + \partial\sigma_{22}/\partial x_2 + \partial\sigma_{32}/\partial x_3 \\ \partial\sigma_{13}/\partial x_1 + \partial\sigma_{23}/\partial x_2 + \partial\sigma_{33}/\partial x_3 \end{bmatrix}$$

where $\mathbf{n} = n_i\mathbf{E}_i$ is the normal to the solid boundary on A_T or A_U.

2.4. Sticking-contact law

As mentioned in the Introduction, we start with the simple case of sticking contact. However, we will use a penalty formulation: a small relative displacement between the contact points S and F is allowed. Hence, the contact constitutive law may be written as follows:[1]

$$\boldsymbol{\sigma}_C = \mathbf{K}_C\boldsymbol{\varepsilon}_C \tag{6}$$

where

$$\mathbf{K}_C = \begin{bmatrix} K_p & 0 & 0 \\ 0 & K_\tau & 0 \\ 0 & 0 & K_\tau \end{bmatrix} \tag{7}$$

is the diagonal penalty matrix; K_p and K_t are penalty coefficients. With the hypotheses of Section 2.1, this constitutive law transforms the contact problem into that of a solid on an elastic foundation.

2.5. *The functional* Π_C

The following functional is defined:

$$\Pi_C = \int_{A_C} \{W_C(\boldsymbol{\varepsilon}_C) + \boldsymbol{\sigma}_C^T[\mathbf{u}_S - \mathbf{u}_F - \boldsymbol{\varepsilon}_C]\}\, dA_C + \int_V \{W(\boldsymbol{\varepsilon}) + \boldsymbol{\sigma}^T[\partial\mathbf{u} - \boldsymbol{\varepsilon}] - \mathbf{F}^T\mathbf{u}\}\, dV - \int_{A_T} \mathbf{T}^T\mathbf{u}\, dA_T - \int_{A_U} \boldsymbol{\sigma}_n^T[\mathbf{u} - \tilde{\mathbf{u}}]\, dA_U \tag{8}$$

In this functional, $\tilde{\mathbf{u}}$ are the displacements imposed on A_U;

$$W_C(\boldsymbol{\varepsilon}_C) = \tfrac{1}{2}\,\boldsymbol{\varepsilon}_C^T\,\mathbf{K}_C\boldsymbol{\varepsilon}_C \tag{9}$$

is the contact strain energy density;

$$W(\boldsymbol{\varepsilon}) = \tfrac{1}{2}\,\boldsymbol{\varepsilon}^T\mathbf{C}\boldsymbol{\varepsilon} \tag{10}$$

is the strain energy density in the solid; $\mathbf{C}$ is Hooke's elastic tensor written in matrix form, so that

$$\boldsymbol{\sigma} = \mathbf{C}\boldsymbol{\varepsilon} \tag{11}$$

In the functional Π_C, the independent fields are $\boldsymbol{\sigma}$, $\boldsymbol{\varepsilon}$, $\mathbf{u}$, $\boldsymbol{\sigma}_C$, $\boldsymbol{\varepsilon}_C$, $\mathbf{u}_C$.

2.6. *Variation of* Π_C

We express that the above functional is stationary: $\delta\Pi_C = 0$.

Taking the variation of Π_C with respect to the independent fields is straightforward. The results are summarized in Table I. It is seen that all the field equations are recovered in the solid as well as on its boundary.

Table 1. Variation of Π_C

Variable	Region	Equation	Interpretation
$\boldsymbol{\varepsilon}_C$	A_C	$\boldsymbol{\sigma}_C = \mathbf{K}_C\boldsymbol{\varepsilon}_C$	Constitutive law at contact
$\boldsymbol{\sigma}_C$	A_C	$\boldsymbol{\varepsilon}_C = \mathbf{u}_S - \mathbf{u}_F$	Compatibility condition at contact
$\mathbf{u}_S$	A_C	$\boldsymbol{\sigma}_C + \boldsymbol{\sigma}_S = 0$	Surface equilibrium at contact
$\boldsymbol{\varepsilon}$	V	$\boldsymbol{\sigma} = \mathbf{C}\boldsymbol{\varepsilon}$	Constitutive law in the solid
$\boldsymbol{\sigma}$	V	$\boldsymbol{\varepsilon} = \partial\mathbf{u}$	Compatibility in the solid
$\mathbf{u}$	V	$\partial\boldsymbol{\sigma} + \mathbf{F} = 0$	Equilibrium in the solid
$\boldsymbol{\sigma}$	A_U	$\mathbf{u} = \tilde{\mathbf{u}}$	Compatibility with the imposed displacements on A_U
$\mathbf{u}$	A_U	$0 = 0$	—
$\mathbf{u}$	A_T	$\boldsymbol{\sigma}_n = \mathbf{T}$	Surface equilibrium on A_T

2.7. The functional Π_{C1}

Let us assume that the following equations:

$$\begin{aligned} \boldsymbol{\varepsilon} &= \partial \mathbf{u} \quad \text{in } V \\ \boldsymbol{\sigma} &= \mathbf{C}\boldsymbol{\varepsilon} \quad \text{in } V \\ \mathbf{u} &= \tilde{\mathbf{u}} \quad \text{on } A_U \end{aligned} \tag{12}$$

are satisfied *a priori.*

Introducing these conditions in Π_C gives a new functional

$$\Pi_{C1} = \int_{A_C} \{W_C(\boldsymbol{\varepsilon}_C) + \boldsymbol{\sigma}_C^T[\mathbf{u}_S - \mathbf{u}_F - \boldsymbol{\varepsilon}_C]\}\, dA_C + \int_V [W(\mathbf{u}) - \mathbf{F}^T\mathbf{u}]\, dV - \int_{A_T} \mathbf{T}^T\mathbf{u}\, dA_T \tag{13}$$

where $W(\mathbf{u})$ is the strain energy density in the solid, expressed as a function of the independent field $\mathbf{u}$.

In the functional Π_{C1}, the independent fields are $\mathbf{u}$, $\boldsymbol{\sigma}_C$, $\boldsymbol{\varepsilon}_C$. It must be noted that $\mathbf{u}_S$ is not an independent field since it is the restriction of $\mathbf{u}$ on A_C. This fact must be taken into account when the variation of Π_{C1} is calculated.

2.8. Variation of Π_{C1}

Expressing the stationarity of Π_{C1} restitutes the field equations that were not satisfied *a priori*, that is,

$$\boldsymbol{\sigma}_C = \mathbf{K}_C\boldsymbol{\varepsilon}_C, \quad \boldsymbol{\varepsilon}_C = \mathbf{u}_S - \mathbf{u}_F, \quad \boldsymbol{\sigma}_C + \boldsymbol{\sigma}_S = 0 \quad \text{on } A_C$$

$$\partial\boldsymbol{\sigma} + \mathbf{F} = 0 \text{ in } V \quad \text{and} \quad \boldsymbol{\sigma}_n = \mathbf{T} \text{ on } A_T$$

2.9 The functional Π_{C2}

A further simplification can be obtained as follows: we assume that, in addition to (12), the constitutive law at the contact is satisfied *a priori*:

$$\boldsymbol{\varepsilon}_C = \mathbf{K}_C^{-1}\boldsymbol{\sigma}_C \quad \text{on } A_C \tag{14}$$

Then, the contact complementary strain energy density is defined as

$$W_C^*(\boldsymbol{\sigma}_C) = \boldsymbol{\sigma}_C^T\boldsymbol{\varepsilon}_C - W_C(\boldsymbol{\varepsilon}_C) \tag{15}$$

where $\boldsymbol{\varepsilon}_C$ is computed by (14). With these conditions, the following functional is obtained:

$$\Pi_{C2} = \int_{A_C} \{\boldsymbol{\sigma}_C^T[\mathbf{u}_S - \mathbf{u}_F] - W_C^*(\boldsymbol{\sigma}_C)\}\, dA_C + \int_V [W(\mathbf{u}) - \mathbf{F}^T\mathbf{u}]\, dV - \int_{A_T} \mathbf{T}^T\mathbf{u}\, dA_T \tag{16}$$

The independent fields are $\mathbf{u}$ and $\boldsymbol{\sigma}_C$. Here again, $\mathbf{u}_S$ is the restriction of $\mathbf{u}$ on A_C.

2.10. Variation of Π_{C2}

Expressing the stationarity of Π_{C2} yields the following natural conditions:

$$\mathbf{u}_S - \mathbf{u}_F = \mathbf{K}_C^{-1}\boldsymbol{\sigma}_C = \boldsymbol{\varepsilon}_C \quad \text{on } A_C \tag{17}$$

$$\boldsymbol{\sigma}_C + \boldsymbol{\sigma}_S = 0 \quad \text{on } A_C \tag{18}$$

$$\partial\boldsymbol{\sigma} + \mathbf{F} = 0 \qquad \text{in } V \tag{19}$$

$$\boldsymbol{\sigma}_n = \mathbf{T} \qquad \text{on } A_T \tag{20}$$

2.11. *The functional* Π_{C3}

The last simplification is to assume that, in addition to (12) and (14), the compatibility condition (17) is satisfied *a priori*. Introducing these conditions in (13) gives

$$\Pi_{C3} = \int_{A_C} W_C(\mathbf{u}_S)\,dA_C + \int_V [W(\mathbf{u}) - \mathbf{F}^T\mathbf{u}]\,dV - \int_{A_T} \mathbf{T}^T\mathbf{u}\,dA_T \tag{21}$$

in which there is only one independent field $\mathbf{u}$.

2.12. *Variation of* Π_{C3}

The stationarity of Π_{C3} gives the following natural conditions:

$$\boldsymbol{\sigma}_C + \boldsymbol{\sigma}_S = 0 \quad \text{on } A_C \tag{22}$$

$$\partial\boldsymbol{\sigma} + \mathbf{F} = 0 \quad \text{in } V \tag{23}$$

$$\boldsymbol{\sigma}_n = \mathbf{T} \quad \text{on } A_T \tag{24}$$

3. CONTACT FINITE ELEMENTS BASED ON MIXED VARIATIONAL PRINCIPLES

3.1. *General formulation*

In the preceding section, four variational principles were obtained. They can be used to develop several types of finite elements. Here we concentrate on the simplest functional Π_{C2} which is sufficient to illustrate the basic features of mixed contact finite elements.

The deformable solid is discretized with classical finite elements (isoparametric, for example):

$$\mathbf{u} = \mathbf{NU}, \quad \boldsymbol{\varepsilon} = \mathbf{BU} \tag{25}$$

where $\mathbf{U}$ are the nodal displacements, $\mathbf{N}$ the interpolation functions and $\mathbf{B}$ their derivatives.

At the contact boundary, we develop contact elements the nodes of which coincide with those of the underlying solid element (Figure 4). Hence, the discretization of $\mathbf{u}_S$ is deduced from that of the solid:

$$\mathbf{u}_S = \mathbf{N}_C\mathbf{U}_C \tag{26}$$

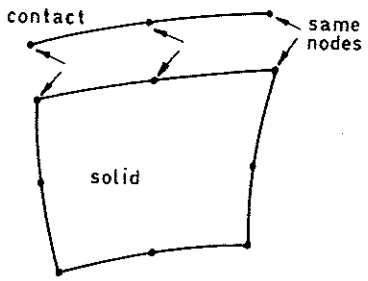

Figure 4

where $\mathbf{U}_C$ are the nodal displacements of the contact element and $\mathbf{N}_C$ are the interpolation functions, obtained by the restriction of $\mathbf{N}$ on the solid element boundary.

Finally, the 'stress' field $\boldsymbol{\sigma}_C$ in the contact element is discretized by

$$\boldsymbol{\sigma}_C = \mathbf{P}\mathbf{q} \tag{27}$$

where $\mathbf{q}$ are contact stress discretization parameters and $\mathbf{P}$ are the corresponding interpolation functions. $\mathbf{q}$ are not necessarily the nodal values of the contact stresses.

The variation of Π_{C2} gives

$$\delta\Pi_{C2} = \int_{A_C} \{\delta\boldsymbol{\sigma}_C^T [\mathbf{u}_S - \mathbf{u}_F] + \boldsymbol{\sigma}_C^T \delta\mathbf{u}_S - \delta\boldsymbol{\sigma}_C^T \mathbf{K}_C^{-1} \boldsymbol{\sigma}_C\} \, dA_C + \int_V [\boldsymbol{\sigma}^T \delta\boldsymbol{\varepsilon} - \mathbf{F}^T \delta\mathbf{u}] \, dV - \int_{A_T} \mathbf{T}^T \delta\mathbf{u} \, dA_T = 0 \tag{28}$$

This variational principle is applied to one solid element and the corresponding contact element. Its discretized form is obtained by introducing (25)–(27) into (28).

The calculation is straightforward. The result is

$$\delta\Pi_{C2} = \delta\mathbf{q}^T \{\mathbf{M}_C\mathbf{U}_C - \boldsymbol{\chi}_C\mathbf{q} - \mathbf{V}_F]\} + \delta\mathbf{U}_C^T\mathbf{M}_C^T\mathbf{q} + \delta\mathbf{U}^T\{\mathbf{K}_S\mathbf{U} - \mathbf{F}_S\} = 0 \tag{29}$$

where

$$\mathbf{M}_C = \int_{A_C} \mathbf{P}^T\mathbf{N}_C \, dA_C \tag{30}$$

$$\boldsymbol{\chi}_C = \int_{A_C} \mathbf{P}^T\mathbf{K}_C^{-1}\mathbf{P} \, dA_C \tag{31}$$

$$\mathbf{V}_F = \int_{A_C} \mathbf{P}^T\mathbf{u}_F \, dA_C \tag{32}$$

$$\mathbf{K}_S = \int_V \mathbf{B}^T\mathbf{C}\mathbf{B} \, dV \tag{33}$$

$$\mathbf{F}_S = \int_V \mathbf{N}^T\mathbf{F} \, dV + \int_{A_T} \mathbf{N}^T\mathbf{T} \, dA_T \tag{34}$$

In these integrals, V is the volume of the solid element and A_T is the surface of its boundary, while A_C is the surface of the contact element. It must be noted that $\mathbf{U}$ and $\mathbf{U}_C$ are not independent, since the nodes of the contact element coincide with some nodes of the solid element. This can be expressed by

$$\mathbf{U}_C = \mathbf{A}\mathbf{U} \tag{35}$$

where $\mathbf{A}$ is an assembly operator. Hence, the independent variables in (29) are $\mathbf{U}$ and $\mathbf{q}$. The coefficient of $\delta\mathbf{q}$ must vanish. Then

$$\mathbf{M}_C\mathbf{U}_C - \boldsymbol{\chi}_C\mathbf{q} - \mathbf{V}_F = 0 \tag{36}$$

This result expresses that the compatibility at contact (17) is satisfied in a weighted-average sense. From (36)

$$\mathbf{q} = \boldsymbol{\chi}_C^{-1}\{\mathbf{M}_C\mathbf{U}_C - \mathbf{V}_F\} \tag{37}$$

Introducing (37) into (29) gives

$$\delta\Pi_{C2} = \delta U_C \{k_C U_C - f_C\} + \delta U^T (K_S U - F_S) = 0 \tag{38}$$

where

$$k_C = M_C^T \chi_C^{-1} M_C \tag{39}$$

$$f_C = M_C^T \chi_C^{-1} V_F \tag{40}$$

Finally, taking account of (35), (38) becomes

$$\delta\Pi_{C2} = \delta U^T \{KU - F_E\} = 0 \tag{41}$$

or

$$KU = F_E \tag{42}$$

where

$$K = K_S + A^T k_C A \tag{43}$$

$$F_E = F_S + A^T f_C \tag{44}$$

It is seen that k_C is the stiffness matrix of the mixed contact element and f_C the corresponding nodal force vector. Equations (43) and (44) represent nothing else than the assembly of the contact element with the corresponding underlying solid element.

For comparison, the formulation of a compatible contact element based on Π_{C3} is explained briefly. The variation of the first term of Π_{C3} gives

$$(\delta\Pi_{C3})_I = \int_{A_C} \delta\varepsilon_C^T K_C \varepsilon_C \, dA_C = \int_{A_C} \delta u_S^T K_C [u_S - u_F] \, dA_C$$
$$= \delta U_C^T [k_C^* U_C - f_C^*] \tag{45}$$

where

$$k_C^* = \int_{A_C} N_C^T K_C N_C \, dA_C \tag{46}$$

$$f_C^* = \int_{A_C} N_C^T K_C u_F \, dA_C \tag{47}$$

are the stiffness matrix of the compatible contact element and the corresponding nodal force vector, respectively.

3.2. *First example*

As a first application, we consider, in the two-dimensional case, a contact element with linear displacement field and constant contact stress field (Figure 5).

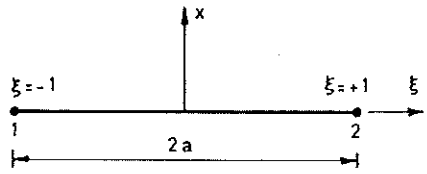

Figure 5

The discretization of the displacement field (22) becomes, here

$$\begin{bmatrix} u_x \\ u_y \end{bmatrix} = \begin{bmatrix} N_1 & 0 & N_2 & 0 \\ 0 & N_1 & 0 & N_2 \end{bmatrix} \begin{bmatrix} U_x^1 \\ U_y^1 \\ U_x^2 \\ U_y^2 \end{bmatrix} \tag{48}$$

with

$$N_1 = \tfrac{1}{2}(1 - \xi); \quad N_2 = \tfrac{1}{2}(1 + \xi) \tag{49}$$

The discretization of the contact stress field (27) becomes

$$\begin{bmatrix} p \\ \tau \end{bmatrix} = \begin{bmatrix} 1 & 0 \\ 0 & 1 \end{bmatrix} \begin{bmatrix} p \\ \tau \end{bmatrix} \tag{50}$$

In this particular case, $\mathbf{q}$ are the constant values of the contact stresses on the element. Assuming, for simplicity, that the motion of the foundation is a translation, one computes successively:

$$\mathbf{K}_C = \begin{bmatrix} K_p & 0 \\ 0 & K_\tau \end{bmatrix}, \quad \chi_C = 2a \begin{bmatrix} 1/K_p & 0 \\ 0 & 1/K_\tau \end{bmatrix}, \quad \mathbf{V}_F = 2a \begin{bmatrix} u_{Fx} \\ u_{Fy} \end{bmatrix}$$

$$\mathbf{M}_C = a \begin{bmatrix} 1 & 0 & 1 & 0 \\ 0 & 1 & 0 & 1 \end{bmatrix}$$

$$\mathbf{k}_C = \frac{a}{2} \begin{bmatrix} K_p & 0 & K_p & 0 \\ 0 & K_\tau & 0 & K_\tau \\ K_p & 0 & K_p & 0 \\ 0 & K_\tau & 0 & K_\tau \end{bmatrix}, \quad \mathbf{f}_C = a \begin{bmatrix} K_p u_{Fx} \\ K_\tau u_{Fy} \\ K_p u_{Fx} \\ K_\tau u_{Fy} \end{bmatrix} \tag{51}$$

On the other hand, if the stiffness matrix (46) and the nodal force vector (47) of a compatible contact element are computed by reduced numerical integration with only one integration point located at $\xi = 0$ (Figure 2), one gets

$$\mathbf{k}_C^* = 2a[\mathbf{N}_C(\xi = 0)]^T \mathbf{K}_C [\mathbf{N}_C(\xi = 0)], \quad \mathbf{f}_C^* = 2a[\mathbf{N}_C(\xi = 0)]^T \mathbf{K}_C \{\mathbf{u}_F(\xi = 0)\}$$

with

$$[\mathbf{N}_C(\xi = 0)] = \frac{1}{2} \begin{bmatrix} 1 & 0 & 1 & 0 \\ 0 & 1 & 0 & 1 \end{bmatrix}, \quad \{\mathbf{u}_F(\xi = 0)\} = \begin{bmatrix} u_{Fx} \\ u_{Fy} \end{bmatrix}$$

An elementary calculation shows that the result is exactly the same as (51). Hence, the mixed contact element with constant stress field is equivalent to the compatible contact element underintegrated with one integration point at $\xi = 0$.

We have seen that (36) expresses the average compatibility at contact. Applying (36) for this example gives

$$\begin{bmatrix} a(U_x^1 - U_x^2) \\ a(U_y^1 - U_y^2) \end{bmatrix} - \begin{bmatrix} 2a\, p/K_p \\ 2a\, \tau/K_\tau \end{bmatrix} - \begin{bmatrix} 2a\, u_{Fx} \\ 2a\, u_{Fy} \end{bmatrix} = 0$$

Hence

$$p = K_p[\tfrac{1}{2}(U_x^1 + U_x^2) - u_{Fx}]$$
$$\tau = K_\tau[\tfrac{1}{2}(U_y^1 + U_y^2) - u_{Fy}]$$

The terms between brackets represent the penetration of the middle point ($\xi = 0$) of the element into the foundation. This is another proof of the equivalence between the mixed contact element and the underintegrated compatible element.

3.3. Second example

We consider a parabolic displacement field and a constant contact stress field (Figure 6). The discretized displacement field is

$$\begin{bmatrix} u_x \\ u_y \end{bmatrix} = \begin{bmatrix} N_1 & 0 & N_2 & 0 & N_3 & 0 \\ 0 & N_1 & 0 & N_2 & 0 & N_3 \end{bmatrix} \begin{bmatrix} U_x^1 \\ U_y^1 \\ U_x^2 \\ U_y^2 \\ U_x^3 \\ U_y^3 \end{bmatrix} \tag{54}$$

with

$$N_1 = \tfrac{1}{2}\xi(1 - \xi), \quad N_2 = 1 - \xi^2, \quad N_3 = \tfrac{1}{2}\xi(1 + \xi) \tag{55}$$

The discretized stress field is given by (50). The stiffness matrix and the nodal force vector are

$$\mathbf{k}_C = \frac{a}{18}\begin{bmatrix} K_p & 0 & 4K_p & 0 & K_p & 0 \\ 0 & K_\tau & 0 & 4K_\tau & 0 & K_\tau \\ 4K_p & 0 & 16K_p & 0 & 4K_p & 0 \\ 0 & 4K_\tau & 0 & 16K_\tau & 0 & 4K_\tau \\ K_p & 0 & 4K_p & 0 & K_p & 0 \\ 0 & K_\tau & 0 & 4K_\tau & 0 & K_\tau \end{bmatrix}; \quad \mathbf{f}_C = \frac{a}{3}\begin{bmatrix} K_p\, u_{Fx} \\ K_\tau\, u_{Fy} \\ 4K_p\, u_{Fx} \\ 4K_\tau\, u_{Fy} \\ K_p\, u_{Fx} \\ K_\tau\, u_{Fy} \end{bmatrix} \tag{56}$$

For this element too, the application of (36) is interesting. After some calculations, one gets

$$p = K_p[\tfrac{1}{6}(U_x^1 + 4U_x^2 + U_x^3) - u_{Fx}]$$
$$\tau = K_\tau[\tfrac{1}{6}(U_y^1 + 4U_y^2 + U_y^3) - u_{Fy}]$$

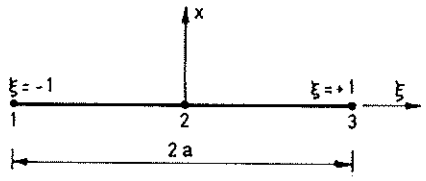

Figure 6

The terms between brackets are the average penetration of the contact element into the foundation. But here they are not the penetration of any particular point of the element, so that this mixed element is not equivalent to any underintegrated compatible element.

3.4. *Third example*

We consider a parabolic displacement field (Figure 6) and a linear constant stress field. The discretized displacement field is given by (54) and (55) and the discretization (27) of the contact stress field gives

$$\begin{bmatrix} p \\ \tau \end{bmatrix} = \begin{bmatrix} P_1 & 0 & P_3 & 0 \\ 0 & P_3 & 0 & P_3 \end{bmatrix} \begin{bmatrix} p_1 \\ \tau_1 \\ p_3 \\ \tau_3 \end{bmatrix} \tag{59}$$

with

$$P_1(\xi) = \tfrac{1}{2}(1 - \xi), \quad P_3(\xi) = \tfrac{1}{2}(1 + \xi) \tag{60}$$

Here $\mathbf{q}$ are the values of p and τ at nodes 1 and 3 of the contact element.

The calculations are straightforward and give

$$\mathbf{k}_C = \frac{a}{9} \begin{bmatrix} 2K_p & 0 & 2K_p & 0 & -K_p & 0 \\ 0 & 2K_\tau & 0 & 2K_\tau & 0 & -K_\tau \\ 2K_p & 0 & 8K_p & 0 & 2K_p & 0 \\ 0 & 2K_\tau & 0 & 8K_\tau & 0 & 2K_\tau \\ -K_p & 0 & 2K_p & 0 & 2K_p & 0 \\ 0 & -K_\tau & 0 & 2K_\tau & 0 & 2K_\tau \end{bmatrix}, \quad \mathbf{f}_C = \frac{a}{3} \begin{bmatrix} K_p & u_{Fx} \\ K_\tau & u_{Fy} \\ 4K_p & u_{Fx} \\ 4K_\tau & u_{Fy} \\ K_p & u_{Fx} \\ K_\tau & u_{Fy} \end{bmatrix}$$

The application of (36) gives

$$\begin{aligned} p_1 &= K_p[\tfrac{1}{3}(2U_x^1 + 2U_x^2 - U_x^3) - u_{Fx}] \\ p_3 &= K_p[\tfrac{1}{3}(-U_x^1 + 2U_x^2 + 2U_x^3) - u_{Fx}] \end{aligned} \tag{61}$$

and similar relations for τ_1 and τ_3.

Is there an equivalent underintegrated compatible contact element? To answer this question, we must search for points ξ such that

$$p(\xi) = K_p[u_x(\xi) - u_{Fx}]$$

with

$$p(\xi) = P_1(\xi)p_1 + P_3(\xi)p_3, \quad u_x = N_1(\xi)U_x^1 + N_2(\xi)U_x^2 + N_3(\xi)U_x^3$$

This gives the equation

$$\begin{aligned} P_1[\tfrac{1}{3}(2U_x^1 + 2U_x^2 - U_x^3) - u_{Fx}] + P_3[\tfrac{1}{3}(-U_x^1 + 2U_x^2 + 2U_x^3] - u_{Fx}] \\ = N_1 U_x^1 + N_2 U_x^2 + N_3 U_x^3 - u_{Fx} \end{aligned}$$

which also writes

$$U_x^1[\tfrac{2}{3}P_1 - \tfrac{1}{3}P_3 - N_1] + U_x^2[\tfrac{2}{3}P_1 + \tfrac{2}{3}P_2 - N_2]$$
$$+ U_x^3[-\tfrac{1}{3}P_1 + \tfrac{2}{3}P_2 - N_3] - u_{Fx}(P_1 + P_2) + u_{Fx} = 0$$

Since $P_1 + P_2 = 1$ for any ξ, this equation is satisfied if the terms between brackets vanish. This happens for

$$\xi = \pm \frac{1}{\sqrt{3}}$$

This means that the mixed contact element developed in this section is equivalent to a parabolic compatible contact element underintegrated with two Gauss points.

3.5. *Fourth example*

The last example is a contact element in which the displacement field and the contact stress field have the same degree. Again, the two-dimensional case and the translation of the foundations are assumed for simplicity. The calculations of $\mathbf{k}_C$ and $\mathbf{f}_C$ are straightforward and are not interesting. However, the application of the average compatibility equation (36) gives again an interesting result. For example, for parabolic fields (3 nodes), one obtains

$$\begin{bmatrix} p_1 \\ p_2 \\ p_3 \end{bmatrix} = K_p \begin{bmatrix} U_x^1 - u_{Fx} \\ U_x^2 - u_{Fx} \\ U_x^3 - u_{Fx} \end{bmatrix}$$

and a similar equation for contact shear stresses τ_1, τ_2, τ_3. This shows that compatibility at contact between solid and foundation is ensured at the nodal points of the mixed contact element. An equivalent compatible element could be obtained by using a numerical integration scheme in which the integration points coincide with the nodes.

4. EXTENSION OF THE THEORY

4.1. *Corotational formulation*

If the solid is submitted to large inelastic strains and if there is sliding with friction at contact, the formulation presented above has to be modified as explained hereafter.

In the solid, the equilibrium is expressed in the current configuration in terms of Cauchy stresses, whether in fixed co-ordinates (which implies the choice of an objective stress rate in the incremental constitutive equation,[8-10] or in a corotational local reference frame rotating with the material particle (which implies the choice of an appropriate spin.[11]) Then, the equilibrium in the current configuration of the solid simply writes

$$\partial\boldsymbol{\sigma} + \mathbf{F} = 0, \quad \boldsymbol{\sigma}_n = \mathbf{T} \tag{62}$$

where the derivatives are taken with respect to the current co-ordinates, $\mathbf{F}$ are body forces per unit current volume and $\mathbf{T}$ are surface traction per unit current area.

At contact, we chose a corotational formulation: the local co-ordinates $\mathbf{e}_1$, $\mathbf{e}_2$, $\mathbf{e}_3$ (Figure 3) rotate with the corresponding surface element.[2] In this local frame, the incremental contact law with sliding and friction writes

$$\dot{\boldsymbol{\sigma}}_C = \mathbf{K}_{CT}\,\dot{\boldsymbol{\varepsilon}}_C \tag{63}$$

with

$$\dot{\varepsilon}_C = \dot{u}_S - \dot{u}_F \tag{64}$$

In (63), the contact constitutive matrix $\mathbf{K}_{CT}$ is usually non-symmetric.[1,2] In the same frame, the equilibrium at contact is

$$\sigma_S + \sigma_C = 0 \tag{65}$$

4.2. Mixed variational equation

In non-linear analysis, the functionals are replaced by variational equations. In particular, Π_{C2} is replaced by

$$\int_{a_C} \sigma_C^T \delta u_S \, da_C + \int_{a_C} [u_S - u_F - \varepsilon_C]^T \delta\sigma_C \, da_C + \int_v [\sigma^T \delta\varepsilon - F^T \delta u] \, dv - \int_{a_T} T^T \delta u \, da_T = 0 \tag{66}$$

where ε_C is a function of σ_C obtained by integration of (63) along the equilibrium path:

$$\varepsilon_C = \int_0^t [K_{CT}]^{-1} \dot{\sigma}_C \, dt \tag{67}$$

and similarly

$$u_S - u_F = \int_0^t [\dot{u}_S - \dot{u}_F] \, dt \tag{68}$$

In (66), the integrals are taken over the current configuration of the solid; δu are virtual displacements and $\delta\varepsilon$ the corresponding virtual strains; $\delta\sigma_C$ are virtual contact stresses. The development of (66) immediately restores the equilibrium equations (62), (65) and the compatibility condition (64). Therefore, the variational equation (66) generalizes the approach of Sections 2.9 and 2.10 to the case of frictional contact between a rigid foundation and an inelastic solid undergoing large strains. The fact that the contact zone a_C is unknown *a priori* is not a special problem because of the step-by-step solution in non-linear analysis. At each iteration, a simple search algorithm[12] is used to determine the current contact surface a_C to be used in the integrals of (66).

4.3. Mixed finite element

Using the same notations as in Section 3.1, the discretization gives

$$\delta u = N \delta U, \quad \delta\varepsilon = B \delta U, \quad \delta\sigma_C = P \delta q; \quad \delta u_S = N_C \delta U_C, \quad \delta U_C = A \delta U$$

With the following definitions

$$F_I = \int_v B^T \sigma \, dv, \quad F_S = \int_v N^T F \, dv + \int_{a_T} N^T T \, da_T$$

$$F_C = \int_{a_C} N_C^T \sigma_C \, da_C, \quad V = \int_{a_C} P^T [u_S - u_F] \, da_C$$

$$E_C = \int_{a_C} P^T \varepsilon_C \, da_C$$

the variational equation (66) gives the discretized equilibrium equation

$$\mathbf{F}_I - \mathbf{F}_S + \mathbf{A}^T \mathbf{F}_C = 0 \tag{69}$$

and the discretized compatibility equation

$$\mathbf{E}_C = \mathbf{V} \tag{70}$$

Both are non-linear functions of the discretization parameters $\mathbf{U}$, $\mathbf{q}$ and of the loading history. Their solution can be obtained by the classical step-by-step method with Newton–Raphson iterations. To this end, the incremental forms of (69) and (70) must be derived. While doing this, we must take care of the fact that v, a_T and a_C are also incremented during a time step. However, the isoparametric concept makes things easy. For example, in the two-dimensional case (contact along a line) we write

$$\mathbf{E}_C = \int_{-1}^{+1} \mathbf{P}^T \boldsymbol{\varepsilon}_C J \, d\xi$$

where J is the Jacobian of the isoparametric transformation.

The increment of J can always be expressed by a relation of the form

$$\dot{J} = \mathbf{G}^T \dot{\mathbf{U}}_C$$

Then

$$\dot{\mathbf{E}}_C = \int_{-1}^{+1} \mathbf{P}^T \dot{\boldsymbol{\varepsilon}}_C J \, d\xi + \int_{-1}^{+1} \mathbf{P}^T \boldsymbol{\varepsilon}_C \dot{J} \, d\xi$$

or

$$\dot{\mathbf{E}}_C = \boldsymbol{\chi}_{CT} \dot{\mathbf{q}} + \mathbf{G}_C \dot{\mathbf{U}}_C$$

with

$$\boldsymbol{\chi}_{CT} = \int_{a_C} \mathbf{P}^T \mathbf{K}_{CT} \mathbf{P} \, da_C, \quad \mathbf{G}_C = \int_{-1}^{+1} \mathbf{P}^T \boldsymbol{\varepsilon}_C \mathbf{G}^T \, d\xi$$

Similarly, we obtain

$$\dot{\mathbf{V}} = \mathbf{M}_C \dot{\mathbf{U}}_C + \mathbf{G}_V \dot{\mathbf{U}}_C - \dot{\mathbf{V}}_F, \quad \dot{\mathbf{F}}_C = \mathbf{M}_C^T \dot{\mathbf{q}} + \mathbf{G}_F \dot{\mathbf{U}}_C$$

with

$$\mathbf{M}_C = \int_{a_C} \mathbf{P}^T \mathbf{N}_C \, da_C, \quad \mathbf{G}_V = \int_{-1}^{+1} \mathbf{P}^T [\mathbf{u}_S - \mathbf{u}_F] \mathbf{G}^T \, d\xi$$

$$\dot{\mathbf{V}}_F = \int_{a_C} \mathbf{P}^T \dot{\mathbf{u}}_F \, da_C, \quad \mathbf{G}_F = \int_{-1}^{+1} \mathbf{N}_C^T \boldsymbol{\sigma}_C \mathbf{G}^T \, d\xi$$

Finally, we write

$$\dot{\mathbf{F}}_I = \mathbf{K}_{ST} \dot{\mathbf{U}}$$

where $\mathbf{K}_{ST}$ is the tangent stiffness matrix of the solid element (see Reference 13 for example), and we assume, for simplicity, that the forces acting on the solid are conservative.

Introducing these results into (70), we obtain

$$\dot{\mathbf{q}} = \boldsymbol{\chi}_{CT}^{-1} [[\mathbf{M}_C + \mathbf{G}_V - \mathbf{G}_C] \dot{\mathbf{U}}_C - \dot{\mathbf{V}}_F] \tag{71}$$

Then, from (69) and (71), we get

$$\mathbf{K}_T \dot{\mathbf{U}} = \dot{\mathbf{F}}_E \tag{72}$$

with

$$\mathbf{K}_T = \mathbf{K}_{ST} + \mathbf{A}^T \mathbf{k}_{CT} \mathbf{A}, \quad \dot{\mathbf{F}}_E = \dot{\mathbf{F}}_S + \mathbf{A}^T \dot{\mathbf{f}}_C \tag{73}$$

where $\dot{\mathbf{f}}_C$ is the incremental nodal force vector of the mixed contact element

$$\dot{\mathbf{f}}_C = \mathbf{M}_C^T \chi_{CT}^{-1} \dot{\mathbf{V}}_F \tag{74}$$

and $\mathbf{k}_{CT}$ is its tangent stiffness matrix

$$\mathbf{k}_{CT} = \mathbf{M}_C^T \chi_{CT}^{-1} \mathbf{M}_C + \mathbf{M}_C^T \chi_{CT}^{-1} [\mathbf{G}_V - \mathbf{G}_C] + \mathbf{G}_F \tag{75}$$

The first term is due to the material non-linearity and the second is due to the geometrical non-linearity, that is the evolution of a_C during the deformation process.

5. APPLICATION

Contact finite elements based on the preceding theory have been implemented in the large-strain finite element code LAGAMINE developed at the M.S.M. department of the University of Liège. In two-dimensional analysis, parabolic line elements with linear contact stress field and rectilinear elements with constant or linear contact stress field were developed. In the three-dimensional case, four-node and eight-node surface elements with constant or bilinear contact stress field are used.

Two applications are given below to illustrate the effectiveness of the method.

5.1. Axisymmetric forging problem

An example of realistic forging is presented showing the validity of the method. We first use 120 PL8LS elements (eight-node isoparametric elements with four integration points) to discretize the workpiece submitted to compression between dies of arbitrary shapes (Figure 7) in axisymmetric state. An elastic–viscoplastic constitutive law for solid elements has been applied with following

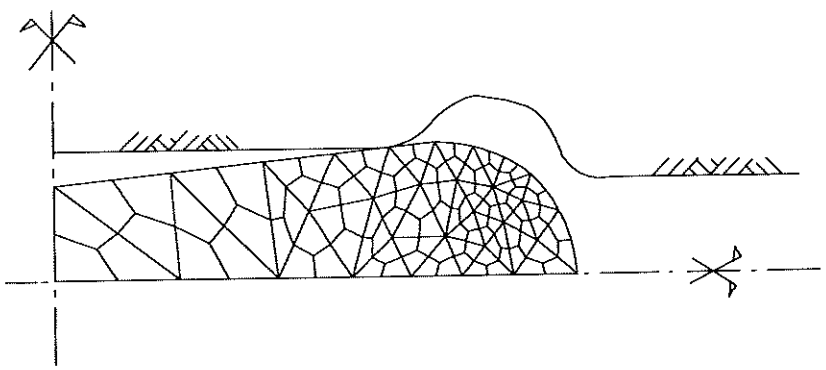

Figure 7. Initial mesh for the forging problem

parameters:

$$F = \frac{\sqrt{J_2}}{K}, \quad J_2 = \tfrac{1}{2}\hat{\sigma}_{ij}\hat{\sigma}_{ij}$$

If $\sqrt{J_2} < K$ then elastic Hooke's law; else

$$\dot{\hat{\sigma}}_{ij} = C_{ijkl}(\dot{\varepsilon}_{kl} - \dot{\varepsilon}^n_{kl})$$

$$\dot{\varepsilon}^n_{ij} = B(F)^r \frac{1}{\sqrt{J_2}} \hat{\sigma}_{ij}$$

where $\dot{\hat{\sigma}}_{ij}$ is the objective derivative of the deviatoric part of the Cauchy stress tensor, $\dot{\varepsilon}_{kl}$ the total strain rate, $\dot{\varepsilon}^n_{kl}$ the inelastic strain rate, $r = 9{\cdot}259$, $B = 0{\cdot}034$, $E = 1{\cdot}2 \times 10^5$ MPa, $\nu = 0{\cdot}4$, $k = \text{const} = 0{\cdot}5 \times 10^5$ MPa, no hardening is considered.

A Coulomb dry friction law has been chosen as the constitutive law for unilateral contact. The simulation has been performed from $t = 0{\cdot}0$ to $7{\cdot}0 \times 10^{-4}$ s, which implies a reduction in height from 0·5316 to 0·3143 cm (40·8 per cent).

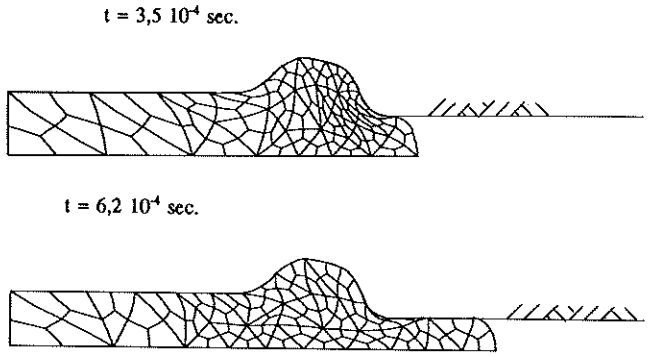

Figure 8. Deformed mesh

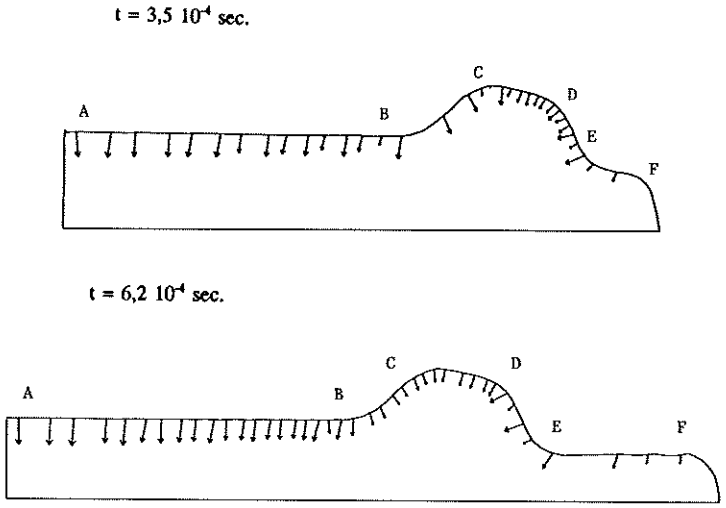

Figure 9. Diagrams of contact stresses

Because of the high distortion of the finite elements, three remeshings have been applied (see References 14 and 15 for more information). The deformed mesh is presented in Figure 8 at two stages, $t = 3{\cdot}48 \times 10^{-4}$ s and $t = 6{\cdot}20 \times 10^{-4}$ s.

The contact stress vectors are presented in Figure 9. They are quite regular under the central and plane part A–B of the tool. But the tool bump modifies dramatically the evolution of the contact. For the first illustrated state ($t = 3{\cdot}5 \times 10^{-2}$ s), some gaps appear on the B–C section. For the later state ($t = 6{\cdot}2 \times 10^{-2}$ s), the same situation holds on the E–F section. Contact exists there only at few integration points and this induces a disturbed diagram of contact pressure and, following the Coulomb friction law, a disturbed diagram of friction stresses.

5.2. *Shear-bond test*

Shear-bond tests are used to predict the nature of the composite interaction between many materials. Advantages of these tests are that they are easy to perform and that the results may easily be incorporated into a theoretical analysis. Here we consider a shear-bond test (called 'push-off' test) for predicting the full-scale behaviour of cold-formed steel–concrete composite slabs. Figure 10 presents a push-off test for composite slabs. Two concrete blocks are cast with

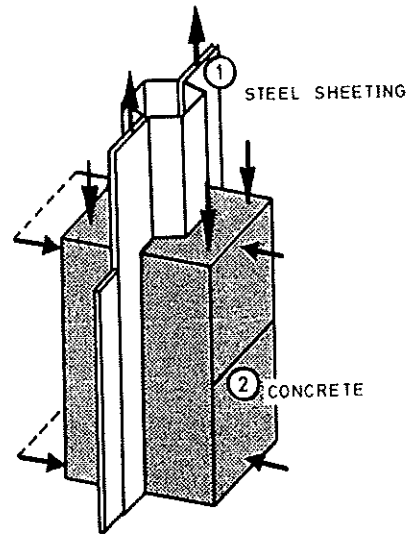

Figure 10. Push-off test for composite slabs

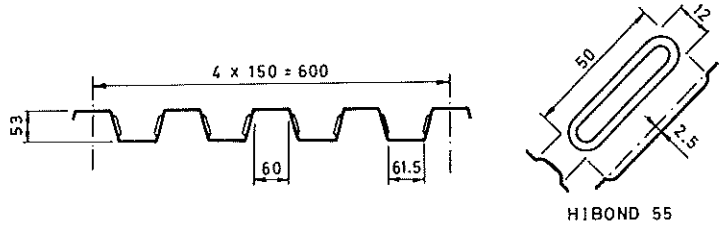

Figure 11. Sheeting geometry: cross-section and embossment pattern

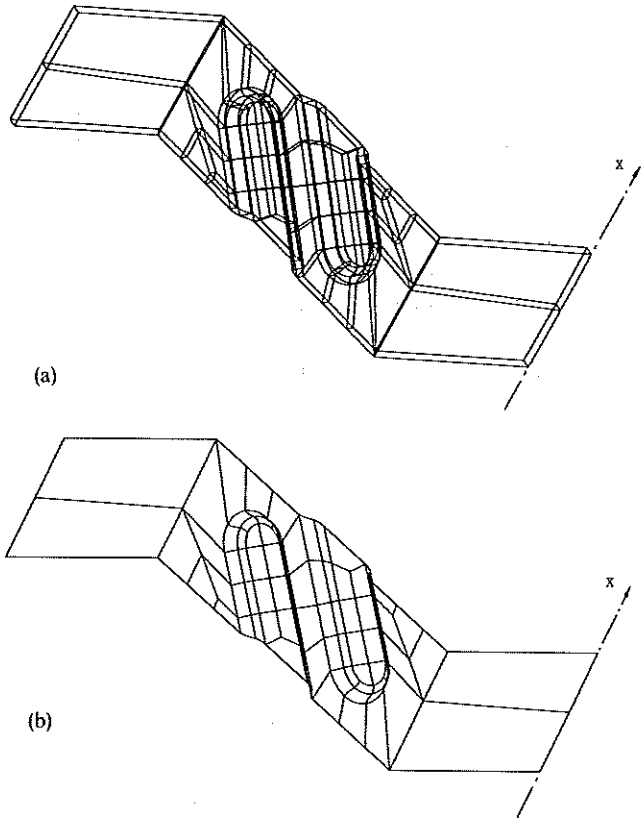

Figure 12. Solid (a) and contact (b) meshes for the shear bond test

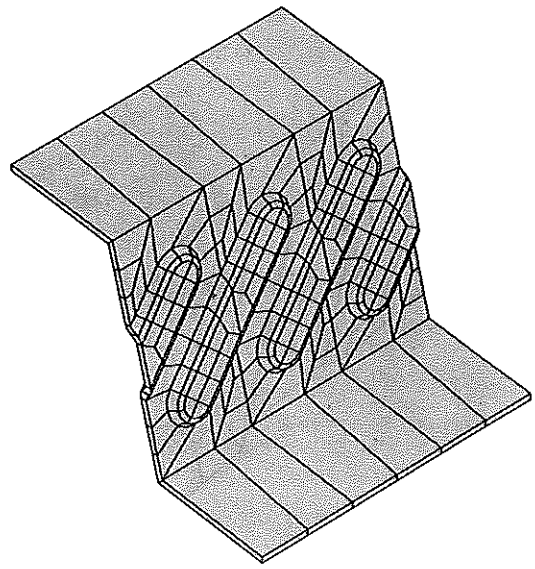

Figure 13. 3-D view of the discretized problem

sheeting placed on opposite faces. The length of sheeting in contact with concrete is generally 300 mm.

Rib geometry and embossments can vary from one steel sheeting to the other. Figure 11 gives the cross-section and the embossment pattern of the profiled sheeting (type HIBOND-55) used in the finite element simulation. The sheeting thickness is equal to 1 mm.

The steel sheeting discretization consists of 88 volume elements of degree two (20 nodes), with one element over the thickness, and 88 contact elements connected with the upper face of the sheeting. Concrete is assumed to be infinitely rigid. It is discretized by a spatial set of 372 triangular segments, representing the foundation of this problem. Figure 12 represent the discretization of the volume and contact elements.

As we want to treat the case of an infinite number of embossments, we have discretized only a small part of the profiled sheeting (two half-embossments), and we have imposed the condition

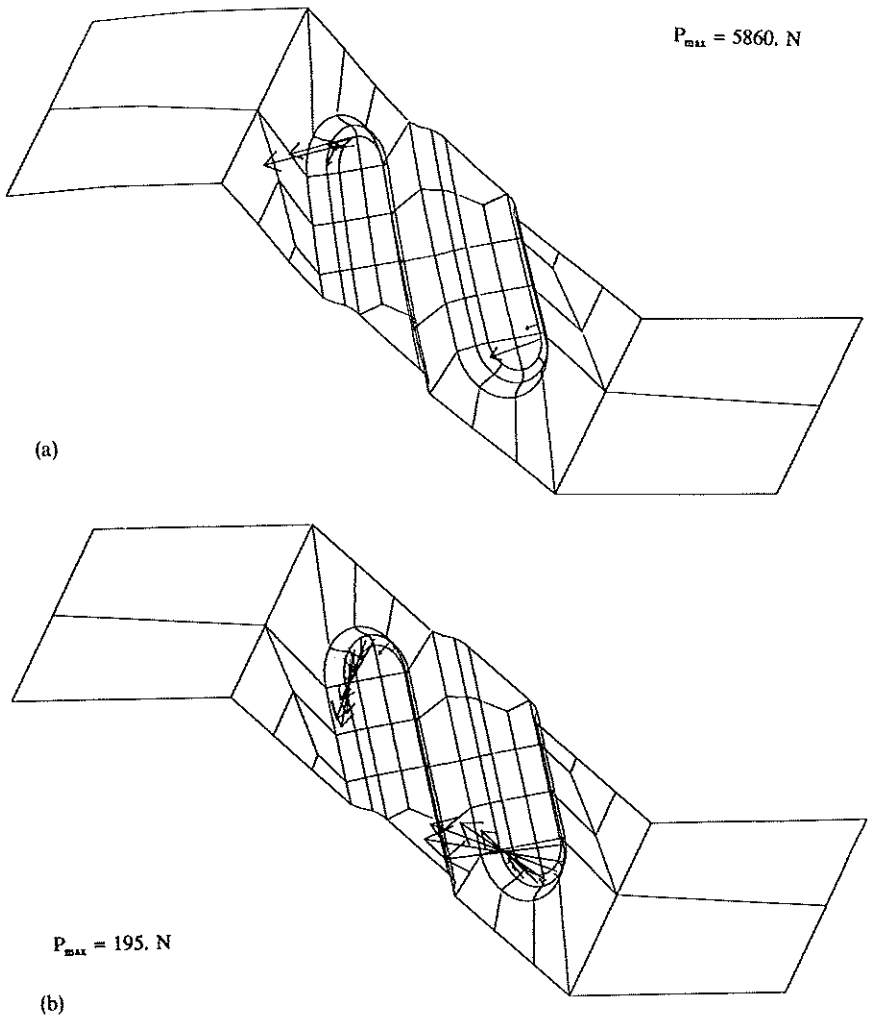

Figure 14. Contact forces (a) 0·0001 mm displacement (b) 4 mm displacement

that nodes along the side X = constant C_1 have the same equations as the corresponding nodes located along the opposite side (X = constant C_2). To have a best sight of the steel sheeting with embossments, we have repeated several times, just for drawing and not for calculation, the studied structure. The result is shown in Figure 13.

The whole foundation is completely fixed and a uniform displacement in the X-direction is imposed on all the nodes along the sides X = constant. We suppose that the steel sheeting remains elastic ($E = 210{\cdot}000$ N/mm^2, $\nu = 0,30$) during the simulation. The contact between concrete and steel is assumed, in first approximation, to be without friction, the coefficients K_ρ and K_τ of the penalty method being equal to 20000 N/mm^3.

The finite element simulation has been carried out till the steel sheeting displacement in the X-direction reaches 4 mm.

Plate 1(a) and 1(b) gives the contact pressures between steel and concrete when the structure displacement in the X-direction equals 10^{-4} and 4 mm, while Figure 14 shows the contact forces for these same displacements. In these figures we can notice that, during the simulation, contact between structure and foundation is concentrated only on the top of embossment's extremities; the steel sheeting comes, therefore, off concrete, contact regions remaining very limited. Plate 1(c) shows the structure deformations after 4 mm displacement.

REFERENCES

1. R. Charlier and S. Cescotto, 'Modélisation du phénomène de contact unilatéral avec frottement dans un contexte de grandes déformations', *J. Theoret. Appl. Mech.* (Special issue, supplément), **7**(1) (1988).
2. R. Charlier, A. Godinas and S. Cescotto, 'On the modelling of contact problems with friction by the finite element method', in *Proc. 8th Conf. on SMIRT*, Brussels, 1985.
3. A. Klarbring and B. Tortenfelt, 'A Newton method for contact problems with friction and interface compliance', in D. R. J. Owen, E. Oñate and E. Hinton, (eds.), *Proc. of COMPLAS İII*, pp. 409–420. Barcelona, April 1992.
4. J. T. Oden and E. B. Pires, Non-local and non linear friction laws and variational principles for contact problems in elasticity. *J. Appl. Mech.*, **50**, 67–76 (1983).
5. J. T. Oden and E. B. Pires, 'Algorithms and numerical results for finite element approximations of contact problems with non-classical friction laws', *Comp. Struct.*, **19**, 137–147 (1984).
6. A. Curnier, A theory of friction. *Int. j. solids struct.*, **20**, 637–647 (1984).
7. C. S. Desai and B. N. Nagaraj, 'Modeling for cyclic normal and shear behavior of interfaces', *J. Eng. Mech., ASCE*, **114**, 1198–1217 (1988).
8. E. H. Lee, R. L. Mallett and T. B. Wertheimer, 'Stress analysis for kinematic hardening of finite deformation plasticity', Stanford University, *SUDAM Report no 81-11*, 1981.
9. J. K. Dienes, 'On the analysis of rotation and stress rate in deforming bodies', *Acta Mechanica*, **32**, 217 (1979).
10. Y. Dafalias, 'Corotational rates for kinematic hardening at large plastic deformation', *J. Appl. Mech.*, **50**, 561–565 (1983).
11. A. Dogui, 'Plasticité anisotrope en grandes déformations', Thèse de doctorat d'Etat présentée devant l'Université Claude Bernard, Lyon 1, 1989.
12. S. Cescotto, 'Computer aided methods for improved accuracy of drop forging tools', BRITE Project No RI1B-0281-C(AM), *Research report no 2*, 1989.
13. S. Cescotto and R. Charlier, 'Numerical simulation of elasto-visco-plastic large strains of metals at high temperature', in *Proc. 8th Conf. on SMIRT*, Brussels, 1985.
14. M. Dyduch and A. M. Habraken, 'Automatic adaptive remeshing for numerical simulation of forging', *Actes de la Conf. Europ. sur les nouvelles avancées en calcul des structures.* 2–5 avril 1991 (Giens), 1991.
15. A. M. Habraken and S. Cescotto, 'An automatic remeshing technique for finite element simulation of forming processes', *Int. j. numer. methods eng.*, **30**, 1503–1525 (1990).
16. A. B. Chandhary and K. J. Bathe, 'A solution method for static and dynamic analysis of three-dimensional contact problems with friction', *Comp. Struct.*, **24**, 855–873 (1986).

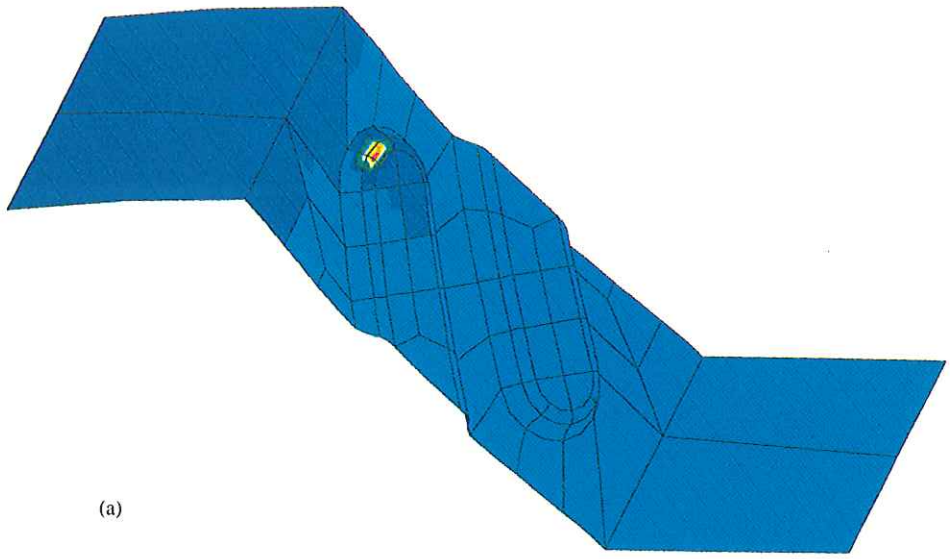

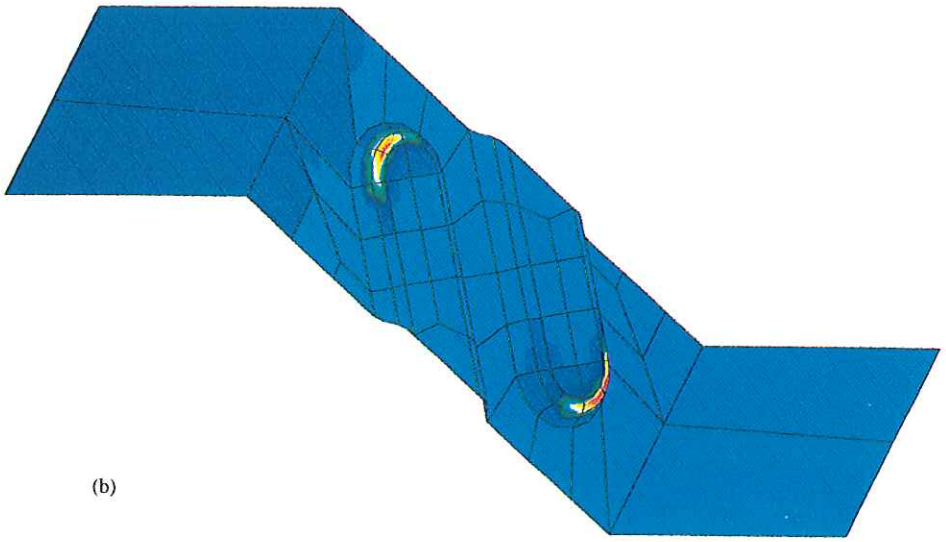

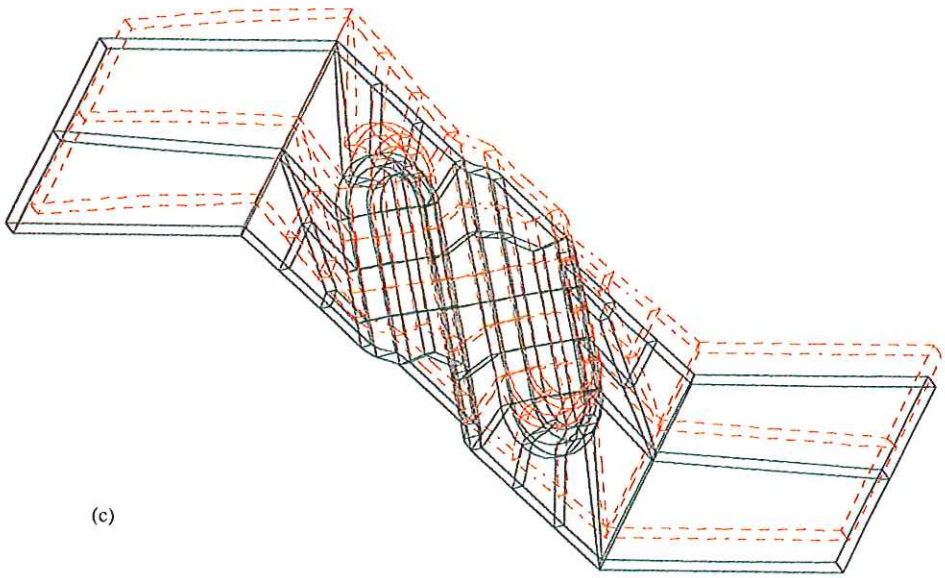

Plate 1 (a) contact pressure after a displacement of 4mm (b) contact pressure after a displacement of 0.0001mm (c) deformed mesh after a displacement of 4mm.